A dynamically young and perturbed Milky Way disk

T. Antoja[1], A. Helmi[2], M. Romero-Gómez[1], D. Katz[3], C. Babusiaux[4], R. Drimmel[5], D. W. Evans[6], F. Figueras[1], E. Poggio[5,7], C. Reylé[8], A.C. Robin[8], G. Seabroke[9], C. Soubiran[10]

[1]Institut de Ciències del Cosmos, Universitat de Barcelona (IEEC-UB), Martí i Franquès 1, E-08028 Barcelona, Spain
[2]Kapteyn Astronomical Institute, University of Groningen, Landleven 12, 9747 AD Groningen, The Netherlands
[3]GEPI, Observatoire de Paris, Université PSL, CNRS, 5 Place Jules Janssen, 92190 Meudon, France
[4]Univ. Grenoble Alpes, CNRS, IPAG, 38000 Grenoble, France
[5]INAF - Osservatorio Astrofisico di Torino, via Osservatorio 20, 10025 Pino Torinese (TO), Italy
[6]Institute of Astronomy, University of Cambridge, Madingley Road, Cambridge CB3 0HA, UK.
[7]Università di Torino, Dipartimento di Fisica, via Pietro Giuria 1, 10125 Torino, Italy
[8]Institut UTINAM, CNRS UMR6213, Univ. Bourgogne Franche-Comté, OSU THETA Franche-Comté Bourgogne, Observatoire de Besançon, BP 1615, 25010 Besançon Cedex, France.
[9]Mullard Space Science Laboratory, University College London, Holmbury St Mary, Dorking, Surrey RH5 6NT, United Kingdom
[10]Laboratoire d'astrophysique de Bordeaux, Univ. Bordeaux, CNRS, B18N, allée Geoffroy Saint-Hilaire, 33615 Pessac, France

Abstract

The evolution of the disk of our Galaxy, which contains most of the stars, has been sculpted by several phenomena. The bar and the spiral arms, for instance, induce radial migration[1] and trapping/scattering of stars close to orbital resonances.[2] External perturbations from satellite galaxies must also play a role, causing dynamical heating,[3] creating rings[4] and correlations between velocities.[5] These perturbations cause phase-wrapping signatures in the disk,[6–9] such as arched velocity structures in the motions of stars in the Galactic plane. Some manifestations of these dynamical processes have been already detected in observations. These include mostly kinematic substructure in samples of nearby stars,[10–12] density asymmetries and velocities across the Galaxy disk that differ from the axisymmetric and equilibrium expectations,[13] especially in the vertical direction,[11,14–16] and signatures of incomplete phase-mixing in the disk.[7,12,17,18] Here we report an analysis of the motions of 6 million stars in the disk of the Milky Way. We show that the phase space distribution is full of substructure with a variety of morphologies, such as snail shells and ridges when spatial and velocity coordinates are combined. We infer that the disk was perturbed between 300 and 900 Myr ago, matching current estimations of the previous pericentric passage of the Sagittarius dwarf galaxy. These findings challenge the most basic premise in stellar dynamics of dynamical equilibrium, and show that modelling the Galactic disk as a time-independent axisymmetric component is definitively incorrect.

Main

Gaia is a cornerstone mission of the European Space Agency (ESA) that has been designed primarily to investigate the origin, evolution and structure of the Milky Way and has just delivered an exquisite product: the largest and most precise census of positions, velocities and other stellar properties for more than a billion stars. By exploring the phase space of more than 6 million stars (positions and velocities) in the disk of the Galaxy in the first kiloparsecs around the Sun from the *Gaia* Data Release[19] 2 (DR2, see Methods), we find that certain phase space projections show plenty of substructures that are new and that had not been predicted by existing models. These have remained blurred until now due to the limitations on the number of stars and the precision of the previously available datasets.

Fig. 1a shows the projection of phase space in the vertical position and velocity Z-V_Z. The stars follow an impressive curled spiral-shaped distribution never seen before whose density increases towards the leading edge of the spiral. Fig. 1b and Fig. 1c show that the "snail shell" is still present when the stars are colour-coded according to their radial and azimuthal velocities, V_R and V_ϕ, implying a strong correlation between the vertical and in-plane motions of the stars. The pattern is particularly pronounced in the V_ϕ colour-coded case (Fig. 1c) even up to $V_Z \sim 40\,\mathrm{km\,s^{-1}}$. Furthermore, we see a gradient with different azimuthal velocities across the spiral shape, following the density variations. Details about the relation between the snail shell and other velocity features observed in the Solar neighbourhood are described in Extended Data Fig. 1.

The spiral shape of Fig. 1a is clearly reminiscent of the effects of phase mixing in two-dimensions discussed in several areas of Astrophysics[20–22] and also in quantum physics[23] but never put in the context of dynamical models of the disk. This process can be better understood with a simple toy model. Consider a Galaxy model whose vertical potential can be approximated by an anharmonic oscillator (see Methods, Eq. 1). In this approximation, the vertical frequencies of oscillation ν depend on the amplitude of the oscillation A and Galactocentric radius R, to first order[22] (see Methods, Eq. 2). By approximating that stars follow a simple harmonic oscillation with these frequencies, their movement with time t is described by $Z = A\cos(\phi(t))$ and $V_Z = -A\nu\sin(\phi(t))$, (being $\phi(t)$ the orbital phase) which traces an oval shape in the clockwise direction in the Z-V_Z projection. However, stars revolve at different angular speeds depending on their frequency. Thus, an ensemble of stars will stretch out in phase space, with the range of frequencies causing a spiral shape in this projection. The detailed time evolution of stars in this toy model is described in Methods and shown in Extended Data Fig. 3. As time goes by, the spiral gets more tightly wound, and eventually, this process of phase mixing leads to a spiral that is so wound that the coarse-grained distribution appears to be smooth. The clarity of the spiral shape in the Z-V_Z plane revealed by the *Gaia* DR2 data, implies that this time has not yet arrived and thus provides unique evidence that phase mixing is currently taking place in the disk of the Galaxy.

This interpretation also implies that the shape of the spiral can be used to obtain information on: i) the shape of the potential, which determines the vertical frequencies, ii) the starting time of the phase mixing, and iii) the type of perturbation that brought the disk to a non-equilibrium state, which sets the initial conditions for the phase mixing event we are witnessing. For instance, we can estimate the time t of the event from the separation between two consecutive spiral turns because these have phase separation of 2π, that is $(\nu_2 t + \phi_{0_2}) - (\nu_1 t + \phi_{0_1}) = 2\pi$, where 1 and 2 indicate two consecutive turns of the spiral. Therefore, we have that $t = \frac{2\pi}{\nu_2 - \nu_1}$, where we have assumed that the initial phase ϕ_{0_i} is the same for 1 and 2. Using several potentials for the Milky Way, as explained in Methods, we estimated that the vertical phase mixing event started about 500 Myr ago, with a likely range of [300, 900 Myr]. A toy model that illustrates this process is shown in Fig. 3a, which depicts a snail shell similar to the data

formed after 500 Myr from an ensemble of stars with a starting distribution that is out of equilibrium.

A possible perturbation that might have sparked the observed on-going vertical phase mixing is the influence of a satellite galaxy. In particular, the last pericentre of the orbit of the Sagittarius dwarf galaxy has been shown to have strong effects on the stellar disk.[4,8,9] In addition, most models locate this pericentric passage between 200 and 1,000 Myr ago,[9,24,25] which is fully consistent with our findings. Nevertheless, other processes that may induce snail shells could be the formation of the central bar and of transient spiral structure, provided that these are able to induce vertical asymmetries, other global changes in the potential, or the dissolution of a massive stellar system such as a cluster or accreted satellite.

Another phase space projection that shows a remarkably different and stunning appearance with the Gaia data is the azimuthal velocity V_ϕ versus cylindric radius R (Fig. 2). Although this phase space projection was explored before with other data,[26] the spatial coverage, high sampling and unprecedented precision of the *Gaia* data unveils a plethora of diagonal thin ridges. The arches in the velocity space projection V_R-V_ϕ at the Solar neighbourhood recently discovered with *Gaia* data[12] and shown in Extended Data Fig. 1a are projections of these diagonal ridges but at a fixed Galactic position. Fig. 2, therefore, reveals that arched structures must be present at many different radii but have remained fully unexplored thus far, and that their characteristics vary with distance from the Galactic centre, diminishing their velocity towards the outskirts of the Galaxy in a continuous way.

These diagonal ridges could be signatures of phase mixing now in the horizontal direction, as has been already predicted for the arches in velocity space.[6–8] Alternatively, the bar and the spiral arms could also induce diagonal ridges created by the resonant orbital structure, which exhibit regions in phase space of stable and unstable orbits,[27] and hence with over-densities and gaps. A simple toy model of phase mixing currently at work (Fig. 3b) but also, a disk simulation with a Galactic potential containing a bar (Fig. 3c) show plenty of diagonal ridges. The V_ϕ velocity separation of consecutive ridges in the data is about $10\,\mathrm{km\,s^{-1}}$. This separation compared to that of all our toy model (see Methods) seems to indicate that if these ridges were caused by phase mixing from a single perturbation, this should have taken place a longer time ago than the one giving rise to the vertical mixing, This conclusion is consistent with the timing derived using the separation between arches in the local velocity plane[7] and some stellar moving groups that appear not to be fully phase mixed vertically,[18] which was found to be 2 Gyr ago. The relation between the various features is not clear, and it is not unlikely that there are/were several perturbations creating superposed features.

Our interpretation of the new features found, however, is based on simple toy models, with their main limitations being the lack of self-consistency, the choice of initial conditions not necessarily reflecting those stemming from the impact of a satellite galaxy, and the fact that we study separately the effects of resonances and phase mixing and also the different dimensions (horizontal and vertical) at play. A challenging task for the future will be to model the new findings taking into account collective effects, such as in the perturbative regime[28] and also with self-consistent N-body models.[25]

References

[1] Sellwood, J. A. & Binney, J. J. Radial mixing in galactic discs. *Mon. Not. R. Astron. Soc.* **336**, 785–796 (2002).

[2] Contopoulos, G. & Grosbol, P. Stellar dynamics of spiral galaxies - Nonlinear effects at the 4/1 resonance. *Astron. Astrophys.* **155**, 11–23 (1986).

[3] Quinn, P. J., Hernquist, L. & Fullagar, D. P. Heating of galactic disks by mergers. *Astrophys. J.* **403**, 74–93 (1993).

[4] Purcell, C. W., Bullock, J. S., Tollerud, E. J., Rocha, M. & Chakrabarti, S. The Sagittarius impact as an architect of spirality and outer rings in the Milky Way. *Nature* **477**, 301–303 (2011).

[5] D'Onghia, E., Madau, P., Vera-Ciro, C., Quillen, A. & Hernquist, L. Excitation of coupled stellar motions in the Galactic Disk by orbiting satellites. *Astrophys. J.* **823**, 4 (2016).

[6] Fux, R. Order and chaos in the local disc stellar kinematics induced by the Galactic bar. *Astron. Astrophys.* **373**, 511–535 (2001).

[7] Minchev, I. *et al.* Is the Milky Way ringing? The hunt for high-velocity streams. *Mon. Not. R. Astron. Soc.* **396**, L56–L60 (2009).

[8] Gómez, F. A., Minchev, I., Villalobos, Á., O'Shea, B. W. & Williams, M. E. K. Signatures of minor mergers in Milky Way like disc kinematics: ringing revisited. *Mon. Not. R. Astron. Soc.* **419**, 2163–2172 (2012).

[9] de la Vega, A., Quillen, A. C., Carlin, J. L., Chakrabarti, S. & D'Onghia, E. Phase wrapping of epicyclic perturbations in the Wobbly Galaxy. *Mon. Not. R. Astron. Soc.* **454**, 933–945 (2015).

[10] Eggen, O. J. Star Streams and Galactic Structure. *Astron. J.* **112**, 1595 (1996).

[11] Dehnen, W. The Distribution of Nearby Stars in Velocity Space Inferred from HIPPARCOS Data. *Astron. J.* **115**, 2384–2396 (1998).

[12] Gaia Collaboration, Katz, D., *et al.* Gaia Data Release 2: Mapping the Milky Way disc kinematics. *Astron. Astrophys.*, DOI 10.1051/0004-6361/201832865 (2018).

[13] Siebert, A. *et al.* Detection of a radial velocity gradient in the extended local disc with RAVE. *Mon. Not. R. Astron. Soc.* **412**, 2026–2032 (2011).

[14] Widrow, L. M., Gardner, S., Yanny, B., Dodelson, S. & Chen, H.-Y. Galactoseismology: Discovery of Vertical Waves in the Galactic Disk. *Astrophys. J.* **750**, L41 (2012).

[15] Schönrich, R. & Dehnen, W. Warp, Waves, and Wrinkles in the Milky Way. *Mon. Not. R. Astron. Soc.* **478**, 3809–3824 (2018).

[16] Quillen, A. C. *et al.* The GALAH Survey: Stellar streams and how stellar velocity distributions vary with Galactic longitude, hemisphere and metallicity. *Mon. Not. R. Astron. Soc.* **478**, 228–254 (2018).

[17] Gómez, F. A. *et al.* Signatures of minor mergers in the Milky Way disc - I. The SEGUE stellar sample. *Mon. Not. R. Astron. Soc.* **423**, 3727–3739 (2012).

[18] Monari, G. *et al.* Coma Berenices: The First Evidence for Incomplete Vertical Phase-mixing in Local Velocity Space with RAVE. Confirmed with Gaia DR2. *Research Notes of the American Astronomical Society* **2**, 32 (2018).

[19] Gaia Collaboration, Brown, A. & et al. Gaia Data Release 2: Summary of the contents and survey properties. *Astron. Astrophys.* DOI 0.1051/0004-6361/201833051 (2018).

[20] Tremaine, S. The geometry of phase mixing. *Mon. Not. R. Astron. Soc.* **307**, 877–883 (1999).

[21] Afshordi, N., Mohayaee, R. & Bertschinger, E. Hierarchical Phase Space Structure of Dark Matter Haloes: Tidal debris, Caustics, and Dark Matter annihilation. *Physical Review D, vol. 79, Issue 8, id. 083526* **79** (2008).

[22] Candlish, G. N. *et al.* Phase mixing due to the Galactic potential: steps in the position and velocity distributions of popped star clusters. *Mon. Not. R. Astron. Soc.* **437**, 3702–3717 (2014).

[23] Manfredi, G. & R. Feix, M. Theory and simulation of classical and quantum echoes. *Physical review. E, Statistical physics, plasmas, fluids, and related interdisciplinary topics* **53**, 6460–6470 (1996).

[24] Law, D. R. & Majewski, S. R. The Sagittarius Dwarf Galaxy: A Model for Evolution in a Triaxial Milky Way Halo. *Astrophys. J.* **714**, 229–254 (2010).

[25] Laporte, C. F. P., Johnston, K. V., Gómez, F. A., Garavito-Camargo, N. & Besla, G. The Influence of Sagittarius and the Large Magellanic Cloud on the Milky Way Galaxy. *Mon. Not. R. Astron. Soc.* DOI 10.1093/mnras/sty1574 (2018).

[26] Monari, G., Kawata, D., Hunt, J. A. S. & Famaey, B. Tracing the Hercules stream with Gaia and LAMOST: new evidence for a fast bar in the Milky Way. *Mon. Not. R. Astron. Soc.* **466**, L113–L117 (2017).

[27] Michtchenko, T. A., Lépine, J. R. D., Barros, D. A. & Vieira, R. S. S. Combined dynamical effects of the bar and spiral arms in a Galaxy model. Application to the solar neighbourhood. *Astron. Astrophys.* DOI 10.1051/0004-6361/201833035 (2018).

[28] Fouvry, J.-B., Binney, J. & Pichon, C. Self-gravity, Resonances, and Orbital Diffusion in Stellar Disks. *Astrophys. J.* **806**, 117 (2015).

Acknowledgements This work has made use of data from the European Space Agency (ESA) mission *Gaia* (`https://www.cosmos.esa.int/gaia`), processed by the *Gaia* Data Processing and Analysis Consortium (DPAC, `https://www.cosmos.esa.int/web/gaia/dpac/consortium`). Funding for the DPAC has been provided by national institutions, in particular the institutions participating in the *Gaia* Multilateral Agreement. This project has received funding from the European Union's Horizon 2020 research and innovation programme under the Marie Skłodowska-Curie grant agreement No. 745617. This work was supported by the MDM-2014-0369 of ICCUB (Unidad de Excelencia 'María de Maeztu') and the European Community's Seventh Framework Programme (FP7/2007-2013) under grant agreement GENIUS FP7 - 606740. AH acknowledges financial support from a VICI grant from the Netherlands Organisation for Scientific Research, NWO. We acknowledge the MINECO (Spanish Ministry of Economy) through grants ESP2016-80079-C2-1-R (MINECO/FEDER, UE) and ESP2014-55996-C2-1-R (MINECO/FEDER, UE). This work has been funded in part by the Agenzia Spaziale Italiana (ASI) through contract 2014-025-R.1.2015 through the Italian Istituto Nazionale di Astrofisica (INAF). EP acknowledges the financial support of the 2014 PhD fellowship programme of INAF.

Author contributions T.A. contributed to the sample preparation, analysed and interpreted the data, performed most of the modelling and wrote the paper together with A.H. A.H. also provided interpretation to the findings. M.R. performed the simulation with the barred potential and contributed to sample preparation. D.K., C.B, R.D., D.W.E, F.F., E.P., C.R., A.C.R, G.S, C.S. contributed to sample preparation and validation of the *Gaia* data. All authors reviewed the manuscript.

Author information Reprints and permissions information is available at www.nature.com/reprints. The authors declare no competing financial interests. Correspondence and requests for materials should be addressed to T.A. (tantoja@fqa.ub.edu).

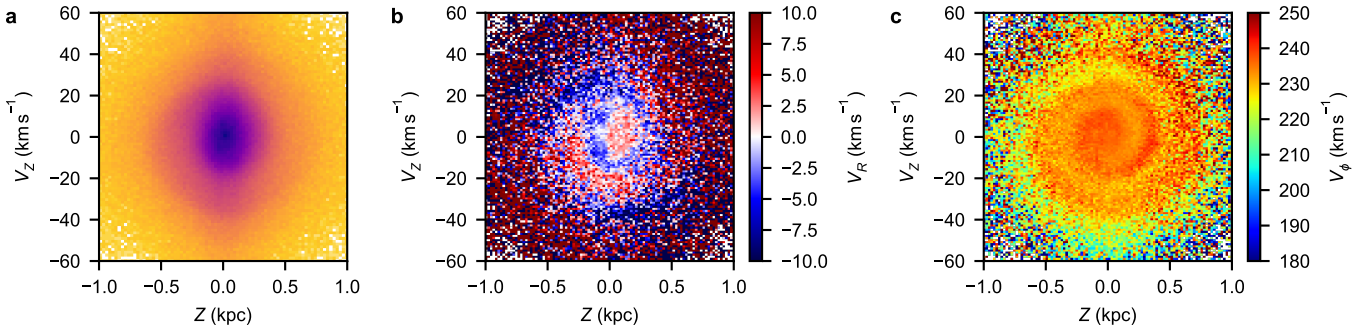

Figure 1: **Vertical positions and velocities of the stars.** The panels show the distribution of stars in the vertical position-velocity plane from our sample of *Gaia* DR2 data for stars with Galactocentric radius $8.24 < R < 8.44$ kpc. a) Two-dimensional histogram in bins of $\Delta Z = 0.01$ kpc and $\Delta V_Z = 0.1\,\mathrm{km\,s^{-1}}$, with the darkness being proportional to the number of counts; b) Z-V_Z plane coloured as a function of median V_R in bins of $\Delta Z = 0.02$ kpc and $\Delta V_Z = 1\,\mathrm{km\,s^{-1}}$; c) Same as b) but for V_ϕ. V_R and V_ϕ are positive towards the Galactic anti-centre and the Galactic rotation direction, respectively.

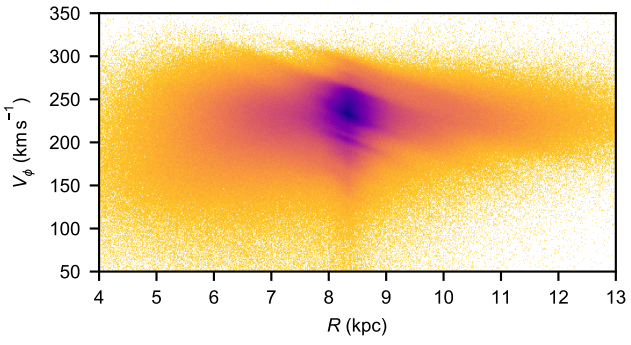

Figure 2: **Positions and velocities of the stars in the disk plane.** Distribution of azimuthal velocities as a function of Galactocentric radius for all stars in our sample with 6D phase space coordinates from *Gaia* DR2 data, built as a two-dimensional histogram in bins of $\Delta V_\phi = 1.\,\mathrm{km\,s^{-1}}$, and $\Delta R = 0.01$ kpc.

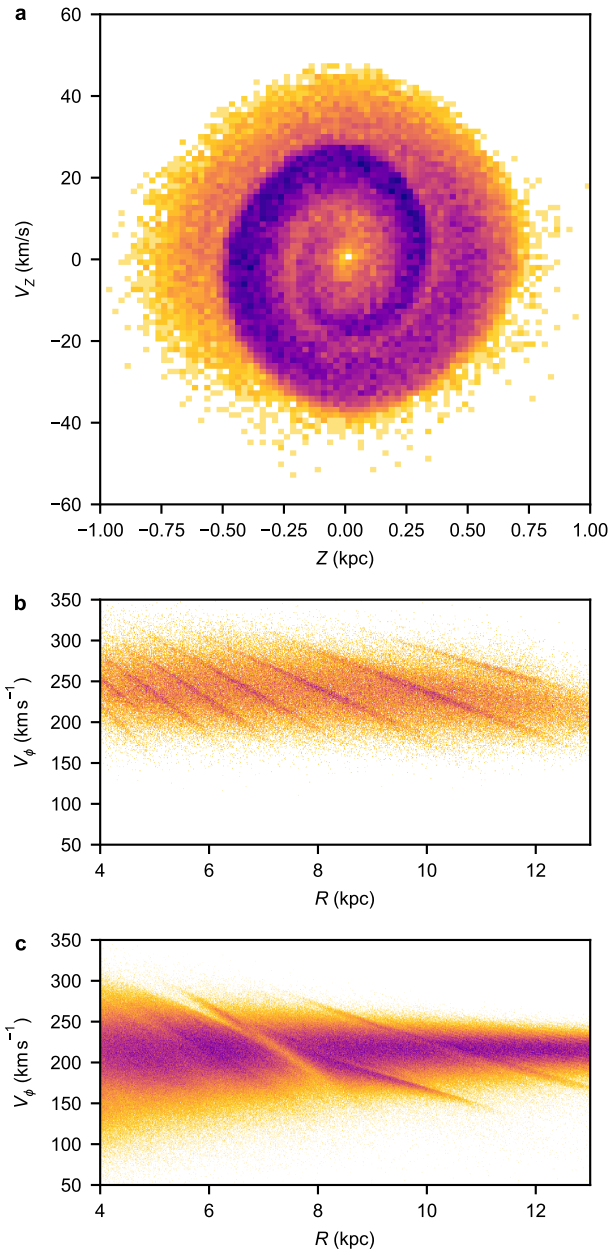

Figure 3: **Models of the phase space distribution of the Galaxy disk.** a) Modelled spiral shape created in the vertical position-velocity plane as a result of the phase mixing in the evolution of an ensemble of particles for 500 Myr in a Galactic potential, starting from a distribution that is out of equilibrium presumably after a certain perturbation; b) Modelled diagonal ridges created in the distribution of azimuthal velocities as a function of Galactocentric radius as a result of the phase mixing in the evolution of an ensemble of particles for 1,000 Myr in a Galactic potential, starting from a distribution that is out of equilibrium; c) Same as b) but for the diagonal ridges created as a result of the effects of the barred potential and its resonant structure. See Methods.

Methods

Data and samples selection

We used *Gaia* DR2 sources for which the 6D phase space coordinates can be computed, that is all sources with available 5 parameters astrometric solution (sky positions, parallax and proper motions) and radial velocities. We selected only stars with positive parallaxes ϖ with relative uncertainty smaller than 20%, i.e. the ones satisfying $\varpi/\sigma_\varpi > 5$. This selection is to ensure that $1/\varpi$ is a reasonably good estimator of the distance to the stars[29] but alternatively, we used also Bayesian distances (see below). This sample has 6,376,803 stars and it has been well studied and characterised elsewhere.[12] The data was obtained directly through the following query in the public *Gaia* Archive (https://gea.esac.esa.int/archive/):

```
SELECT G.source_id, G.radial_velocity, G.radial_velocity_error,
G.ra, G.ra_error, G.dec, G.dec_error, G.parallax, G.parallax_error,
G.pmra, G.pmra_error, G.pmdec, G.pmdec_error,
G.ra_dec_corr, G.ra_parallax_corr, G.ra_pmra_corr, G.ra_pmdec_corr,
G.dec_parallax_corr, G.dec_pmra_corr, G.dec_pmdec_corr,
G.parallax_pmra_corr, G.parallax_pmdec_corr, G.pmra_pmdec_corr
FROM gaiadr2.gaia_source G
WHERE G.radial_velocity IS NOT Null AND G.parallax_over_error>5.
```

From the 5 parameter astrometric solution and line-of-sight velocities ($\alpha, \delta, \varpi, \mu^*_\alpha, \mu_\delta, V_{los}$) of these stars, we derived distances (as $1/\varpi$), positions and velocities in the cylindrical Galactic reference frame, that is (R, ϕ, Z, V_R, V_ϕ, V_Z). For convenience, we took ϕ positive in the direction of Galactic rotation and with origin at the line Sun-Galactic Centre. For these transformations, we adopted a vertical distance of the Sun above the plane of[30] 27 pc, a distance of the Sun to the Galactic centre[31] $R_\odot$ of 8.34 kpc and a circular velocity at the Sun radius of[31] $V_C(R_\odot) = 240$ km s^{-1}. We assumed a peculiar velocity of the Sun with respect of the Local Standard of Rest of[32] $(U_\odot, V_\odot, W_\odot) = (11.1, 12.24, 7.25)$ km s^{-1}. Our choice of values gives $(V_C(R_\odot) + V_\odot)/R_\odot = 30.2$ km s^{-1} kpc^{-1}, which is compatible with the reflex motion of Sgr A*.[33] To derive the uncertainties in these coordinates, we propagate the full covariance matrix. The median errors in the V_R, V_ϕ, V_Z velocities are 1.4, 1.5, and 1.0 km s^{-1}, respectively, and 80% of stars have errors smaller than 3.3, 3.7, 2.2 km s^{-1} in these velocities. The positions in the Cartesian coordinates X-Y and X-Z of the sample are shown in Extended Data Fig. 2.

For part of our study, we selected from our sample the 935,590 stars located in the solar Galactic cylindrical ring, that is with Galactocentric radius $8.24 < R < 8.44$ kpc (dotted lines in Extended Data Fig. 2). For this selection, the median errors in the V_R, V_ϕ, V_Z velocities are 0.5, 0.8, and 0.6 km s^{-1}, respectively, and 80% of stars have errors smaller than 1.1, 2.0, 1.3 km s^{-1} in these velocities.

We note that the velocity uncertainties are significantly smaller than the sizes of the substructures detected and that, together with the number of stars in our samples, this is what made possible their detection. Although there are some correlations between the astrometric *Gaia* observables,[34] these are not responsible for the correlations and substructure seen in our phase space plots. This is because the stars in our sample are distributed through all sky directions, and the phase space coordinates come from combinations of astrometric measurements and radial velocities, in different contributions depending on the direction on the sky. Besides, the astrometric correlations for our sample are small (smaller than

0.2 in their absolute value for more than 50% of stars) and this, combined with the small errors, makes their contribution nonsignificant.

Alternatively, we used distances determined through a Bayesian inference method using the existing implementation in TOPCAT,[35] taking the mode of the posterior distribution and a prior of an exponentially decreasing density of stars with scale length of 1.35 kpc.[36] We found that the differences between this distance determination and the inverse of the parallax are between -2% and 0.6% for 90% of the 6,376,803 stars with $\varpi/\sigma_{\varpi} > 5$, which was expected for small relative errors in parallax. Consequently, the phase space diagrams presented here vary only at pixel level. These panels do not vary even when using the set of 7,183,262 of stars with available radial velocities that include stars with larger parallax errors and stars with negative parallaxes, for which the estimator of the inverse of the parallax would yield unphysical distances. When using another alternative set of Bayesian distances specifically derived for stars from Gaia DR2 with radial velocities using a different prior,[37] we found the differences between these distances and the inverse of the parallax to be between -9% and 5% for 90% of the stars, thus slightly larger than before, but again with no noticeable effects on the phase space panels examined here.

Models for the vertical phase mixing

We first reproduced the spiral shape observed in the Z-V_Z plane with the *Gaia* DR2 data by using a simple toy model. Often the classic harmonic oscillator is employed to describe the vertical movement of stars in galaxy disks under the epicyclic theory.[38] However, in this approximation, which is valid only for very small amplitude orbits for which the potential changes little vertically, stars have the same vertical oscillatory frequency ν and there is no phase mixing, unless orbits at different guiding radius, thus with different frequencies, are considered. Instead, we used an anharmonic oscillator with the potential of the shape

$$\Phi(Z) \propto -\alpha_0 + \frac{1}{2}\alpha_1 Z^2 - \frac{1}{4}\alpha_2 Z^4. \tag{1}$$

We took the coefficients $\alpha_0, \alpha_1, \alpha_2$ corresponding to the expansion for small Z, derived elsewhere,[22] of a Miyamoto-Nagai potential[39] with values of $a = 6.5$ kpc, $b = 0.26$ kpc, $M = 10^{11}$ $M_{\odot}$. These coefficients α depend on Galactocentric radius R, since the vertical pull depends on the distance to the Galactic center. In this anharmonic potential, the frequencies of oscillation are described by

$$\nu(A, R) = \alpha_1(R)^{1/2}\left(1 - \frac{3\alpha_2(R)A^2}{8\alpha_1(R)}\right) \tag{2}$$

where $\nu_0 \equiv \alpha_1^{1/2}$ is the vertical frequency in the epicyclic approximation.

Given an initial distribution of stars $Z(t = 0)$ and $V_Z(t = 0)$, the vertical amplitudes of the orbits can be derived through the conservation of energy and using the fact that at the vertical turn-around point of the orbit ($V_Z = 0$), the (vertical) kinetic energy is null.[22] Assuming that stars follow a simple harmonic oscillation (but with different frequencies), the movement of the stars with time is described by

$$Z = A\cos\left(\nu(A, R)t + \phi_0\right), \qquad V_Z = -A\nu(A, R)\sin\left(\nu(A, R)t + \phi_0\right), \tag{3}$$

where the initial phase of the stars $\phi_0 \equiv \phi(t = 0)$ is obtained from the initial distribution of Z and V_Z and the corresponding amplitudes.

The phase space evolution described above is shown in the top row of Extended Data Fig. 3. Initially, the particles followed a Gaussian distribution in $Z(t = 0)$ and in $V_Z(t = 0)$ with mean and dispersion of -0.1 kpc and 0.04 kpc, and $-2\,\mathrm{km\,s^{-1}}$ and $1\,\mathrm{km\,s^{-1}}$, respectively. We located all particles at the same Galactocentric radius $R = 8.5$ kpc, and thus, they all move under the same functional form of the vertical potential. The initial conditions are shown in Extended Data Fig. 3a, where we colour-coded the particles according to their period. Following Eq. 3, each star follows a clockwise rotation in the Z-V_Z plane. However, they do it at a different angular speed: stars with smaller period located at the closer distances from the mid-plane ($Z = 0$) revolve faster than those located at the largest distances from the mid-plane. The whole range of frequencies is what creates, therefore, the spiral shape. Extended Data Fig. 3b shows the evolution of the system for three initial phases of the time evolution when the spiral shape begins to form. Extended Data Fig. 3c shows the spiral shape after 1,000 Myr of evolution.

In the *Gaia* data (Fig. 1), we do not see a thin spiral but a thick one, with many of the stars in the volume participating in it. A similar effect was reached with our toy model when we included particles at different radius for which the vertical potential changes and the range of amplitudes/frequencies also changes. In Extended Data Fig. 3 (bottom row) we let a similar system evolve as in the top row but starting with initial radius following a skewed normal distribution, which creates a density decreasing with radius as in galaxy disks, with skewness of 10, location parameter of 8.4 kpc and scale parameter of 0.2 kpc. The spiral structure is now thickened similarly to the data, with higher density of stars at the leading edge of the spiral.

To estimate the time of the phase mixing event from the spiral seen in the *Gaia* data (Fig. 1) using

$$t = \frac{2\pi}{\nu_2 - \nu_1}, \tag{4}$$

we needed to locate two consecutive turns of the spiral and estimate their vertical frequencies from their amplitudes and mean radius. For this, we used Extended Data Fig. 5 which has been colour coded as a function of median guiding radius. This was approximated as $R_g \sim \frac{V_\phi R_\odot}{V_c(R_\odot)}$, under the hypothesis of a flat rotation curve, where we used the values of $R_\odot = 8.34$ kpc and $V_c(R_\odot) = 240\,\mathrm{km\,s^{-1}}$ assumed in the coordinate transformation of the data. In this panel we see that the density gradient across the spiral shape is created by stars with different guiding radius that arrive at the solar neighbourhood due to their different amplitudes of (horizontal) radial oscillation. To determine two consecutive turns of the spiral, we focused on stars at the turn-around points ($V_Z = 0$) near the leading edges of the spiral. By visual inspection, we determined an approximate range of Z in which the turn around points are located in Extended Data Fig. 5, concentrating on red colours, for which the spiral is well defined. The ranges of the turn around points are marked with vertical lines and listed, together with the middle value, in Table 1. For these turn-around points, the amplitudes are simply $A = Z$ and from the colour bar we note that the median R_g is around 8.2 kpc. Small changes in this value do not change significantly our final determination of the time of the perturbation.

To estimate the vertical orbital frequencies of these turn-around points, we could not use the toy model presented above since it is valid only for oscillations with small amplitude A, in particular smaller than the vertical scale b of the potential ($A << 0.26$ kpc). Therefore, we took the model of Allen & Santillan[40] with updated parameters that fit current estimations such as for the Sun Galactocentric radius and the circular velocity curve.[41] We computed the vertical frequency numerically in a grid of different radius and vertical amplitudes by integrating orbits and measuring their vertical periods (Extended Data Fig. 4a). The vertical frequency can change along the orbits for stars with large eccentricities in

the horizontal direction, but here for simplicity we put all particles on near circular orbits. We estimated the vertical frequency at each turn-around position directly by interpolating the numbers of Extended Data Fig. 4a using the estimated values for the amplitude and radius.

Finally, taking each pair of turning points, we obtained an estimation of the time since the perturbation using Eq. 4. As an example, the two turning points (amplitudes) of the left part of the spiral are located at -0.59±9 and -0.23±5 kpc, respectively. These correspond to vertical frequencies of $0.058^{+-0.002}_{--0.002}$ and $0.072^{+-0.002}_{--0.002}$ rad Myr^{-1} for $R_g = 8.2$ kpc, which gives a time of 461^{+183}_{-105} Myr. We repeated the same procedure for the second pair of consecutive turning points and also for the edges of the spiral at $Z = 0$ (mid-plane points), which have $V_Z = A\nu$, estimating the frequencies by interpolating the values of Extended Data Fig. 4b. The mid-plane positions are marked as horizontal lines in Extended Data Fig. 5. All results are summarised in Table 1 and Table 2. The mean of the three time estimations is 510 Myr and the minimum and maximum times from the uncertainty ranges are 356 and 856 Myr.

We tested the dependence of our time determination on the potential model used by using a different model.[42] Compared to our previous model, this one has different shape for the halo, disks and bulge, a different total mass and includes thin and thick disks as well as two gas disks. The frequencies in this model are on average smaller by 4% and smaller than 6% for 90% of the points in the grid of Fig. 4a. By repeating the whole process to determine the perturbation time, we obtained 528 Myr with minimum and maximum times from the uncertainty ranges of 361 and 899 Myr, thus, very similar to our previous determination.

We note that our determination is subject to several approximations, namely that we used the vertical frequencies of orbits with conditions of circularity on the plane and for certain assumed Galactic potential models, we considered a unique guiding radius, and we took equal initial phases for the turn-around and mid-plane points.

We finally run a simulation (Fig. 3a) by integrating 100,000 test particle orbits in the updated Allen & Santillan model with initial vertical positions and velocities following Gaussian distributions centred at $Z = -0.4$ kpc and $V_Z = -5$ km s^{-1} and dispersions of 0.15 kpc and 2. km s^{-1}, respectively. Horizontally in the disk plane, they were distributed following a skewed normal in radius R with scale parameter of 0.8 kpc, location parameter of 8, skewness of 10, and all particles at an azimuthal angle $\phi = 0$. The horizontal velocities were set to 0 for the radial component and to the circular velocity at the particle's radius and $Z = 0$ for the azimuthal one. These are initial conditions of circularity on the Galactic plane but not necessarily for orbits with large excursions in Z. The particles orbits were integrated forwards in time for 500 Myr as estimated from the data. We note that this is not meant to be a fit to the data since we have not explored all possible initial configurations that could lead to a similar spiral shape. We see, though, that an initial distribution asymmetric in Z with most particles located at positive or negative Z is required to obtain a single spiral instead of a symmetrical double one.

Model for the horizontal phase mixing

We used a simple toy model to reproduce the diagonal ridges observed in the $V_\phi - R$ plane (Fig. 3b). This model is built by integrating orbits in the Galactic potential of Allen & Santillan[40] with updated parameters that fit current estimations such as for the Sun Galactocentric radius or the circular velocity curve.[41] We used as initial conditions a set of test particles distributed in Galactocentric radius according to a skewed normal distribution with skewness of 10, location parameter of 4 kpc and scale parameter of 6 kpc. The azimuthal angle was fixed between 0 and 50 deg to mimic a localized perturbation in the disk. For simplicity, all particles were put at the mid-plane with null vertical velocities.

The radial and azimuthal velocities were initialised, respectively, following Gaussian distributions centred at 0 with dispersion of $40\,\mathrm{km\,s^{-1}}$ and centred at the circular velocity at the particular radius with a dispersion of $30\,\mathrm{km\,s^{-1}}$. The particle orbits were computed for 1 Gyr. To these particles we added particles in the disk that have been integrated for a much longer timescale and thus that are well-mixed, to simulate the stellar populations that have not been perturbed. Of all the particles in the simulation, we used only the ones located in a range of 10° in azimuthal angle, similar to the data.

Model for the horizontal resonances

The model of Fig. 3c is from a test particle simulation of orbits integrated in a Galactic potential model including a bar.[43] The axisymmetric part of the potential was the Allen & Santillan model.[40] The Galactic bar potential was built using Ferrers ellipsoids[44] oriented with its semi-major axes at 20° from the Sun-Galactic centre line, and its pattern speed was set to 50 $\mathrm{km\,s^{-1}\,kpc^{-1}}$, which corresponds to a period of about 120 Myr. The simulation consisted of 68 million test particles with an initial radial velocity dispersion of $30\,\mathrm{km\,s^{-1}}$ at the Solar radius. Their orbits were first integrated in the axisymmetric potential model for 10 Gyr until they were approximately fully phase mixed. Next, the bar potential was grown in $T_{\mathrm{grow}} \equiv 4$ bar rotations. More details on the bar potential, initial conditions and integration procedure are specified elsewhere.[43] Here we used the final conditions after T_{grow} (~ 500 Myr) and 8 additional bar rotations ($\sim 1,000$ Myr). From all the particles in the simulation, we used only the ones located in a range of 10° in azimuthal angle centred on the Sun, similar to the data.

Additional references

[29] Luri, X. & et al. Gaia Data release 2. Using Gaia parallaxes. *Astron. Astrophys.* DOI 10.1051/0004-6361/201832964 (2018).

[30] Chen, B. *et al.* Stellar Population Studies with the SDSS. I. The Vertical Distribution of Stars in the Milky Way. *Astrophys. J.* **553**, 184–197 (2001).

[31] Reid, M. J. *et al.* Trigonometric Parallaxes of High Mass Star Forming Regions: The Structure and Kinematics of the Milky Way. *Astrophys. J.* **783**, 130 (2014).

[32] Schönrich, R. Galactic rotation and solar motion from stellar kinematics. *Mon. Not. R. Astron. Soc.* **427**, 274–287 (2012).

[33] Reid, M. J. & Brunthaler, A. The Proper Motion of Sagittarius A*. II. The Mass of Sagittarius A*. *Astrophys. J.* **616**, 872–884 (2004).

[34] Lindegren, L. *et al.* Gaia Data Release 2. The astrometric solution. *Astron. Astrophys.* DOI 10.1051/0004-6361/201832727 (2018).

[35] Taylor, M. B. TOPCAT & STIL: Starlink Table/VOTable Processing Software. In Shopbell, P., Britton, M. & Ebert, R. (eds.) *Astronomical Data Analysis Software and Systems XIV*, vol. 347 of *Astronomical Society of the Pacific Conference Series*, 29 (2005).

[36] Astraatmadja, T. L. & Bailer-Jones, C. A. L. Estimating Distances from Parallaxes. II. Performance of Bayesian Distance Estimators on a Gaia-like Catalogue. *Astrophys. J.* **832**, 137 (2016).

[37] McMillan, P. J. Simple distance estimates for Gaia DR2 stars with radial velocities. *Research Notes of the American Astronomical Society* **2**, 51 (2018).

[38] Binney, J. & Tremaine, S. *Galactic Dynamics: Second Edition* (Princeton University Press, 2008).

[39] Miyamoto, M. & Nagai, R. Three-dimensional models for the distribution of mass in galaxies. *PASJ* **27**, 533–543 (1975).

[40] Allen, C. & Santillan, A. An improved model of the galactic mass distribution for orbit computations. *Rev. Mexicana Astron. Astrofis.* **22**, 255–263 (1991).

[41] Irrgang, A., Wilcox, B., Tucker, E. & Schiefelbein, L. Milky Way mass models for orbit calculations. *Astron. Astrophys.* **549**, A137 (2013).

[42] McMillan, P. J. The mass distribution and gravitational potential of the Milky Way. *Mon. Not. R. Astron. Soc.* **465**, 76–94 (2017).

[43] Romero-Gómez, M., Figueras, F., Antoja, T., Abedi, H. & Aguilar, L. The analysis of realistic stellar Gaia mock catalogues - I. Red clump stars as tracers of the central bar. *Mon. Not. R. Astron. Soc.* **447**, 218–233 (2015).

[44] Ferrers, N. On the potentials of ellipsoids, ellipsoidal shells, elliptic laminae and elliptic rings of variable densities. *QJ Pure Appl. Math* **14**, 1–22 (1877).

[45] Eggen, O. J. Stellar groups. II. The ζ Herculis, ϵ Indi and 61 Cygni groups of high-velocity stars. *Mon. Not. R. Astron. Soc.* **118**, 154 (1958).

[46] Blaauw, A. Remarks on Local Structure and Kinematics. In Becker, W. & Kontopoulos, G. I. (eds.) *The Spiral Structure of our Galaxy*, vol. 38 of *IAU Symposium*, 199 (1970).

[47] Skuljan, J., Hearnshaw, J. B. & Cottrell, P. L. Velocity distribution of stars in the solar neighbourhood. *Mon. Not. R. Astron. Soc.* **308**, 731–740 (1999).

[48] Antoja, T., Figueras, F., Fernández, D. & Torra, J. Origin and evolution of moving groups. I. Characterization in the observational kinematic-age-metallicity space. *Astron. Astrophys.* **490**, 135–150 (2008).

Data availability statement The datasets used and analysed for the current study are derived from the data available in the public *Gaia* Archive, [https://gea.esac.esa.int/archive/]. The Bayesian distances for the Gaia sources with radial velocity[37] are available at `http://www.astro.lu.se/~paul/GaiaDR2_RV_star_distance.csv.gz`. The rest of datasets and toy models generated and/or analysed are available from the corresponding author on reasonable request.

Code availability statement We have made use of standard data analysis tools in Python environment. The codes to generate the toy models, simulations and compute orbital frequencies are available from the corresponding author on reasonable request. The code used to compute the orbits for the McMillan 2017 potential[42] is available at https://github.com/PaulMcMillan-Astro/GalPot. The code to compute Bayesian distances from parallaxes is available in the TOPCAT platform.[35]

Extended Data

Extended Data Tables

Extended Data Table 1: **Time estimations from the turn-around points of the spiral.**

Z (kpc)		ν (rad/Myr)	Time (Myr)
-0.59	±5	$0.058^{+0.002}_{0.002}$	461^{+183}_{-105}
-0.23	±5	$0.072^{+0.002}_{0.002}$	
0.40	±5	$0.065^{+0.003}_{0.003}$	566^{+290}_{-140}
0.75	±5	$0.054^{+0.001}_{0.001}$	

The first column indicates the vertical positions of the turn-around points, which are equal to the amplitude of the orbits except for the sign, and the estimated uncertainty ranges. The following columns are the frequencies corresponding to these amplitudes, and the starting times of the phase mixing process corresponding to each pair of consecutive spiral turns.

Extended Data Table 2: **Time estimations from the mid-plane points of the spiral.**

A_{V_Z} ($km\,s^{-1}$)		ν (rad/Myr)	Time (Myr)
-37	±3	$0.066^{+0.002}_{0.002}$	505^{+253}_{-132}
-19	±3	$0.079^{+0.002}_{0.002}$	

The first column indicates the vertical velocities at the mid-plain passages, which are equal to the velocity amplitudes of the orbits except for the sign, and the estimated uncertainty ranges. The following columns are the frequencies corresponding to these amplitudes, and the starting time of the phase mixing process corresponding to the pair of consecutive spiral turns.

Extended Data Figures

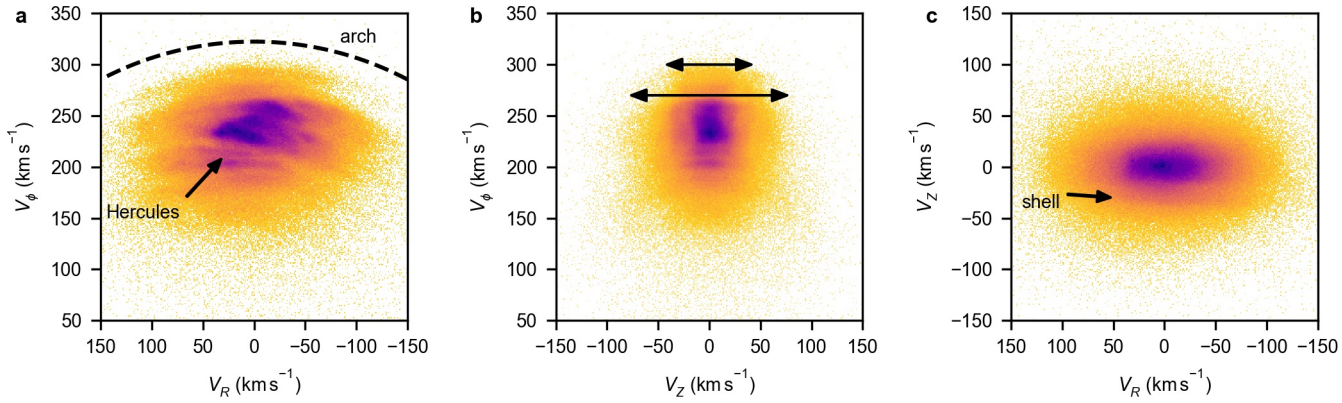

Extended Data Figure 1: **Velocities of the stars at the solar Galactocentric radius.** Two-dimensional histograms of combinations of radial, azimuthal and vertical Galactic cylindrical velocities for the stars in our sample of *Gaia* DR2 data located at $8.24 < R < 8.44$ kpc, in bins of $1\,\mathrm{km\,s^{-1}}$. V_R and V_ϕ are positive towards the Galactic anti-centre and the Galactic rotation direction, respectively. The darkness is proportional to the number of counts. a) Although the bimodality seen in this panel, separating the Hercules stream from the rest of the distribution was known,[45,46] as well as some other elongated structures in this velocity projection[11,47,48] the numerous and thin arches in this panel are a new phenomenon revealed by *Gaia* elsewhere.[12] The semi-circular dotted line in this panel marks an arbitrary line of constant kinetic energy in the plane $E_k = \frac{1}{2}(V_R^2 + V_\phi^2)$, as predicted for the substructure generated in horizontal phase mixing.[7,8] b) This panel depicts a rather boxy appearance, where the extent of the arches in V_Z, varies with their V_ϕ (arrows), likely created by the correlation between the spiral shape and the V_ϕ velocities of Fig. 1c. c) While some velocity asymmetries where noticed before in the $V_\phi - V_Z$ projection[11] and attributed to the Galaxy warp, the sharp shell-like features involving the V_Z velocities, especially at $V_Z \sim -30\,\mathrm{km\,s^{-1}}$ and $V_Z \sim 25\,\mathrm{km\,s^{-1}}$ in this panel, are unveiled here for the first time. These shells are different projections of the snail shell pattern of Fig. 1a.

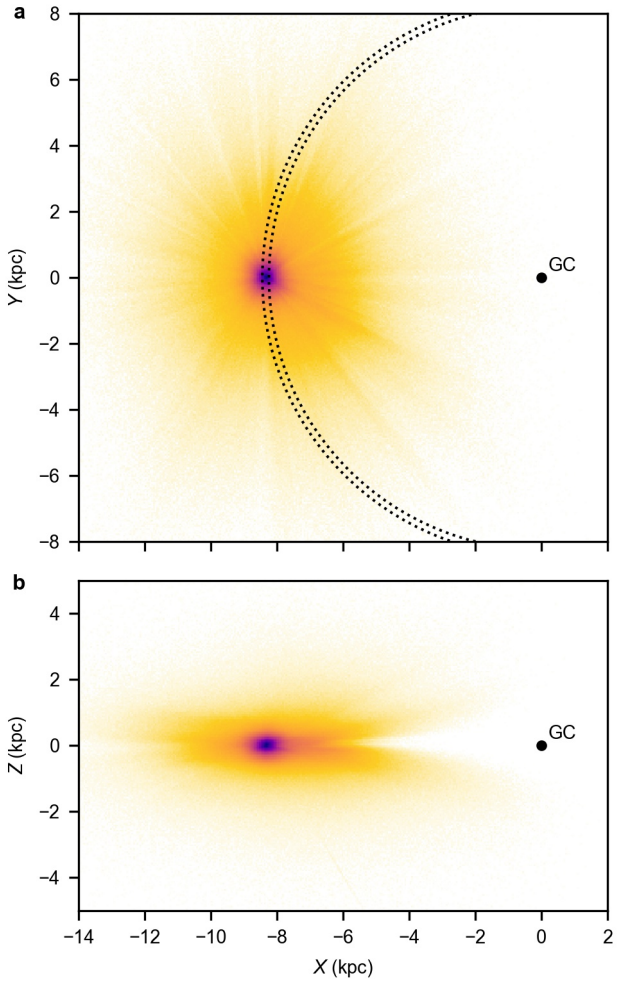

Extended Data Figure 2: **Location of the stars of the sample.** Two dimensional histograms with bins of 0.05 kpc in the X-Y and X-Z projections of our sample of *Gaia* DR2 data. The dotted lines mark the selection of stars in the solar Galactic ring between radius of $[8.24, 8.44]$ kpc. The Sun is located at $(X, Y, Z) = (-8.34, 0., 0.027)$ kpc and the Galactic Centre is marked with a black dot.

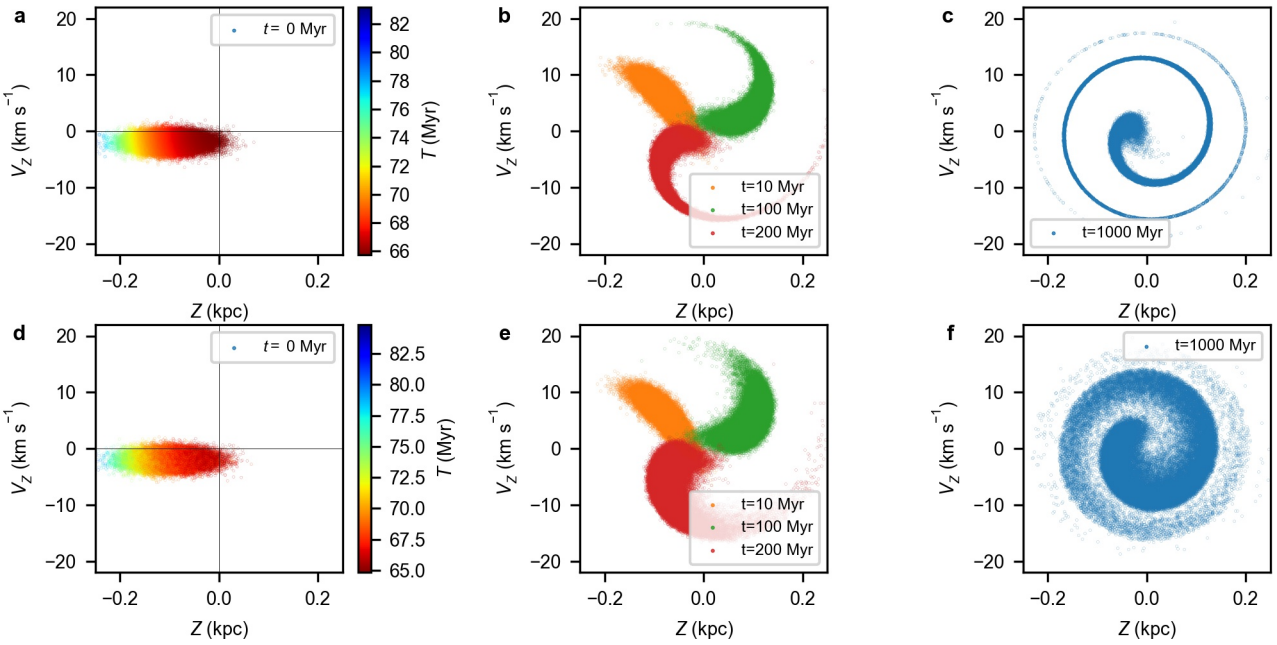

Extended Data Figure 3: **Modelled vertical positions and velocities of stars with time.** The panels show the snail shells created in the phase space evolution under an anharmonic potential. a-b-c) Phase space evolution at different times (t=0, 10, 100, 200, 1,000 Myr) for an ensemble of particles at a fixed Galactocentric radius of $R = 8.5$ kpc with an initial Gaussian distributions in $Z(t = 0)$ with mean of -0.1 kpc and dispersion of 0.04 kpc and in $V_Z(t = 0)$ with mean of -2 km s^{-1} and dispersion of 1 km s^{-1}. d-e-f) Same as a-b-c) but for a skewed normal distribution of initial radius with skewness of 10, location parameter of 8.4 kpc and scale parameter of 0.2 kpc. In both rows, the evolution is the one under an anharmonic oscillator derived from the expansion of a Miyamoto-Nagai disk for small Z. In panels a) and d) the stars are colour coded by vertical period.

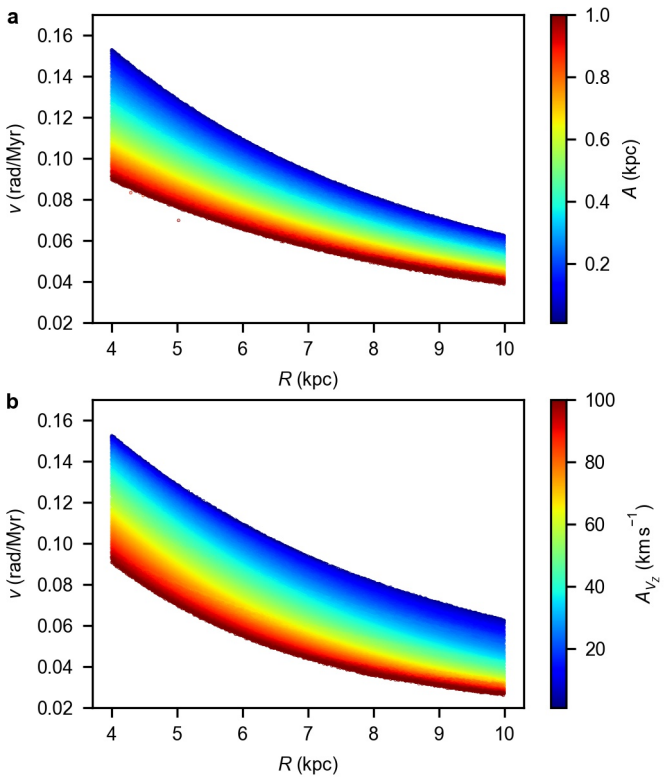

Extended Data Figure 4: **Vertical frequency for orbits in a Galaxy model potential.** Frequencies as a function of Galactocentric radius R computed in the updated Allen & Santillan model[41] a) colour coded by vertical amplitude of the orbits and b) colour coded by vertical velocity amplitude of the orbits.

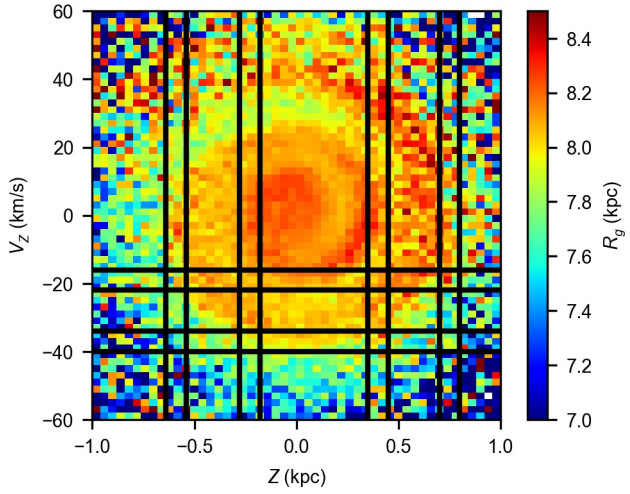

Extended Data Figure 5: **Position of the spiral turns in the vertical positions and velocities.** Z-V_Z plane coloured as a function of median guiding radius R_g for stars at Galactocentric radius of [8.24,8.44] kpc in bins of $\Delta Z = 0.04$(kpc) and $\Delta V_Z = 2\,\mathrm{km\,s^{-1}}$ with horizontal and vertical lines showing the approximate locations of the observed snail shell (turn-around and mid-plane points).